Reading the phase of a Raman excitation with a multi-state atomic interferometer

P. Lombardi,[1,3,4,*] **F. Schaefer,**[1] **I. Herrera,**[1] **S. Cherukattil,**[1] **J. Petrovic,**[2] **C. Lovecchio,**[3] **F. Marin,**[3] **and F. S. Cataliotti**[1,3,4]

[1]*European Laboratory for Nonlinear Spectroscopy (LENS), Via Nello Carrara 1, 50019 Sesto F.no (FI), Italy*

[2]*Vinča Institute of Nuclear Sciences, PO Box 522, 11001 Belgrade, Serbia*

[3]*Dipartimento di Fisica e Astronomia Università di Firenze via Sansone 1, 50019 Sesto F.no (FI), Italy*

[4]*CNR-INO, L.go E. Fermi 2, 50125 Firenze, Italy*

[*]*lombardi@lens.unifi.it*

Abstract: Atomic memories for flying photonic qubits are an essential ingredient for many applications like e.g. quantum repeaters. Verification of the coherent transfer of information from a light field to an atomic superposition is usually obtained using an optical read-out. In this paper we report the direct detection of the atomic coherence by means of atom interferometry. We experimentally verified both that a bichromatic laser field closing a Raman transition imprints a distinct, controllable phase on the atomic coherence and that it can be recovered after a variable time delay.

OCIS codes: (020.1335) Atom optics, (020.1475) Bose-Einstein condensates, (020.1670) Coherent optical effects, (210.4680) Optical memories

References and links

1. H. J. Briegel, W. Dür, J. I. Cirac, and P. Zoller, "Quantum repeaters: The role of imperfect local operations in quantum communication," Phys. Rev. Lett. **81**, 5932–5935 (1998).
2. H. Kimble, "The quantum internet," Nature **453**, 1023–1030 (2008).
3. D. P. DiVincenzo, "Quantum computation," Science **270**, 255–261 (1995).
4. M. A. Nielsen and I. L. Chuang, *Quantum Computation and Quantum Information* (Cambridge University, 2010).
5. A. Mair, J. Hager, D. F. Phillips, R. L. Walsworth, and M. D. Lukin, "Phase coherence and control of stored photonic information," Phys. Rev. A **65**, 031802 (2002).
6. M. Eisaman, A. André, F. Massou, M. Fleischhauer, A. Zibrov, and M. D. Lukin, "Electromagnetically induced transparency with tunable single-photon pulses," Nature **438**, 837–841 (2005).
7. K. Jensen, W. Wasilewski, H. Krauter, T. Fernholz, B. M. Nielsen, M. Owari, M. B. Plenio, A. Serafini, M. M. Wolf, and E. S. Polzik, "Quantum memory for entangled continuous-variable states," Nature Phys. **7**, 13–16 (2011).
8. M. Hosseini, G. Campbell, B. M. Sparkes, P. K. Lam, and B. C. Buchler, "Unconditional room-temperature quantum memory," Nature Phys. **7**, 794–798 (2011).
9. C. Liu, Z. Dutton, C. H. Behroozi, and L. V. Hau, "Observation of coherent optical information storage in an atomic medium using halted light pulses," Nature **409**, 490–493 (2001).
10. C.-W. Chou, J. Laurat, H. Deng, K. Choi, H. De Riedmatten, D. Felinto, and H. Kimble, "Functional quantum nodes for entanglement distribution over scalable quantum networks," Science **316**, 1316–1320 (2007).
11. S. L. Christensen, J. B. Béguin, H. L. Sørensen, E. Bookjans, D. Oblak, J. H. Müller, J. Appel, and E. S. Polzik, "Toward quantum state tomography of a single polariton state of an atomic ensemble," New J. Phys. **15**, 015002 (2013).
12. S. L. Christensen, J. B. Béguin, E. Bookjans, H. L. Sørensen, J. H. Müller, J. Appel, and E. S. Polzik, "Quantum interference of a single spin excitation with a macroscopic atomic ensemble," arxiv: [quant-ph] 1309.2514v2 (2013).
13. J. Petrovic, I. Herrera, P. Lombardi, F. Schaefer, and F. S. Cataliotti, "A multi-state interferometer on an atom chip," New J. Phys. **15**, 043002 (2013).

#205748 - $15.00 USD Received 29 Jan 2014; revised 3 Apr 2014; accepted 5 Apr 2014; published 31 Jul 2014

14. F. Minardi, C. Fort, P. Maddaloni, M. Modugno, and M. Inguscio, "Time-domain atom interferometry across the threshold for Bose-Einstein condensation," Phys. Rev. Lett. **87**, 170401 (2001).
15. R. J. Cook, and B. Shore, "Coherent dynamics of N-level atoms and molecules. III. An analytically soluble periodic case," Phys. Rev. A **20**, 539 (1979).
16. D. M. Harber, H. J. Lewandowski, J. M. McGuirk, and E. A. Cornell, "Effect of cold collisions on spin coherence and resonance shifts in a magnetically trapped ultracold gas," Phys. Rev. A **66**, 053616 (2002).

1. Introduction

High efficiency and high fidelity quantum memories are essential ingredients of both quantum networks [1, 2] and quantum computing schemes [3, 4]. Optical quantum memories have been realized exploiting Raman and electromagnetically induced transparency 3-level schemes in thermal [5, 6, 7, 8] and cold atomic gases [9, 10]. The general approach to assessing the coherence of the information transfer is via optical read-out schemes. Till now only one procedure for a direct detection of the coherence of an atomic quantum memory has been reported [11, 12]. This method does not suffer from the inherent loss mechanism in the transfer of a quantum state between light and atoms, resulting in a better protection of non-classical properties of the state.

Here, we present a tool for the assessment of the atomic coherence that is based on a multi-state atom interferometer. It measures the phase imprinted on quantum degenerate atoms by a bichromatic coherent light field closing a Raman transition. In this way we can directly observe the stored state and measure its decoherence time.

2. Description of the method

We have recently realized a multi-state interferometer that is fully integrated on an atom chip and exploits ^{87}Rb degenerate sample held in a magnetic trap [13]. Our interferometer relies on the internal degree of freedom given by the orientation manifold of a hyperfine ground state. It is based on different responses of the Zeeman states to external fields such as the local magnetic field amplitude or the polarization and intensity of an off-resonant light beam. Our atomic interferometric protocol follows a Ramsey-like procedure (see Fig. 1(a)): two electromagnetic pulses resonant with the magnetic dipole transition connecting adjacent spin-orientation states are applied to the sample one after the other. The first pulse creates a coherent distribution of the atoms in the Zeeman manifold while the second pulse closes the interferometer mapping the relative phases accumulated between the different internal states into a population distribution (as, e.g., in [14]). After the second pulse a Stern-Gerlach procedure is applied. A magnetic field gradient causes the spatial separation of the various Zeeman states. This allows for a simultaneous measurement of the population in each of the possible output states of the interferometer. In [13] we have demonstrated that our five-state interferometer (obtained by choosing the $F = 2$ hyperfine manifold) yields a 1.75 times higher resolution (defined as the ratio between the fringe period and the fringe width) than an ideal two-state interferometer.

In order to obtain a reading of the phase written on the atomic spin by a light field, we used a bichromatic classical light pulse which closes a two-photon Raman transition between adjacent m_F states within the $F = 2$ hyperfine state. For this task we used a coherent source close to the D2 line of the ^{87}Rb ($^2S_{1/2} \rightarrow ^2P_{3/2}$, $\lambda \sim 780$ nm), whose frequency is set 18 GHz to the red of the atomic resonance. We have closed the interferometer by subsequently applying a radio frequency (RF) pulse connecting the same sublevels as the bichromatic field.

The mathematical representation of the experimental sequence follows the lines of Ref. [13]. The effect of a coupling pulse, be it an RF or coherent light (Raman) pulse, is described by a transfer matrix $R(\Omega\tau)$, where Ω and τ represent the Rabi frequency and the duration of the coupling, respectively. The matrix R is obtained by diagonalization of the tridiagonal Hamiltonian which describes the coupling between neighboring m_F states (Ref. [15]). The evolution of the

#205748 - $15.00 USD Received 29 Jan 2014; revised 3 Apr 2014; accepted 5 Apr 2014; published 31 Jul 2014

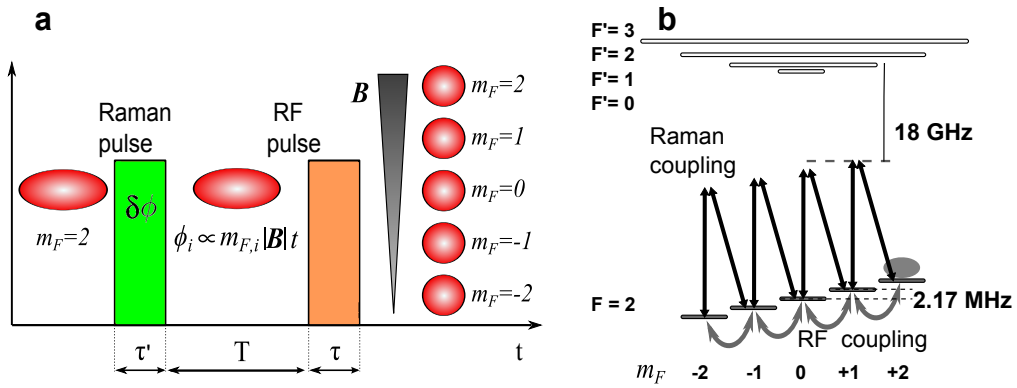

Fig. 1. a) Experimental sequence. The condensate consists of atoms in $|F=2,\, m_F=+2\rangle$ state. Upon release from the magnetic trap the atomic cloud is left free to fall in the homogeneous bias magnetic field **B**. After 100 μs the Raman coupling is applied for a time $\tau' = 6.2$ μs. The resultant superposition of spin levels is left free to evolve for a time $T \sim 1-100$ μs during which atoms in different m_F states acquire differential phases ϕ_i. Then the RF coupling is applied (pulse duration $\tau = 8.3$ μs), followed by the application of a magnetic field gradient to spatially separate the different m_F states. Finally, the population distribution is detected by absorption imaging. b) Energy levels of the $D2$ line of ^{87}Rb (vertical energy axis not to scale) and field couplings used in the experiment.

states in the time interval T between the pulses is described by a diagonal operator P of shape $P_{n,n} = exp[i(n-1)\Delta E/\hbar\ T]$, where we use the index n to refer to the sub-levels of the Zeeman manifold $(n = 1,...,5)$ and ΔE represents, in linear approximation, the Zeeman splitting of neighboring m_F states (see Fig. 1(b)). The full interferometric sequence is then described by a transfer matrix J,

$$J = R(\Omega\tau)\,P(T)\,R(\Omega'\tau')\,,$$

$$J_{j,k} = \sum_{l=1}^{5} R_{j,l}(\Omega\tau)\,e^{i(l-1)\frac{\Delta E}{\hbar}T}\,R_{l,k}(\Omega'\tau')\,, \tag{1}$$

where Ω (Ω') and τ (τ') represent the Rabi frequency and the duration of the RF (Raman) coupling.

The two pulses are chosen such as to have a Rabi area A equal to the optimal value for an interferometer sequence [13], so that $\Omega'\tau' = \Omega\tau e^{i\delta\phi} = Ae^{i\delta\phi}$, where $\delta\phi$ is the relative phase between the two components of the Raman light pulse.

A variation of $\delta\phi$ has no effect on the resulting distribution of populations after a single pulse, but imprints a different phase on the coherences between the wave function components. Indeed, after the Raman coupling, the atomic state consists of the Zeeman components with relative phases following $\phi_{n+1} - \phi_n = \delta\phi$, where ϕ_n is the phase of the n^{th} wave function component, and the index n is still used to refer to the sub-levels of the manifold. Accordingly, the experimental sequence Eq. (1) can be rewritten as

$$J_{j,k} = \sum_{l=1}^{5} R_{j,l}(A)\,e^{i(l-1)\frac{\Delta E}{\hbar}\left(T+\frac{\hbar}{\Delta E}\delta\phi\right)}\,R_{l,k}(A)\,. \tag{2}$$

From Eq. (2), it is evident that the dependence on the phase of the Raman coupling $\delta\phi$ is formally equivalent to the effect of an additional evolution time of the coherent superposition

#205748 - $15.00 USD Received 29 Jan 2014; revised 3 Apr 2014; accepted 5 Apr 2014; published 31 Jul 2014

of the Zeeman states as described by the operator P for a time delay $T'(\delta\phi)$,

$$T'(\delta\phi) = \frac{\hbar}{\Delta E}\delta\phi\,. \tag{3}$$

Therefore, while in our previous work a fringe-like behavior of the population distribution as a function of the delay time T is observed, in the present experiment, we expect to observe the same oscillation as a function of the imprinted phase $\delta\phi$ for a fixed T.

3. Experimental set-up and results

The initial state of the experiment is a pure condensate in the $|F=2,m_F=2\rangle$ state. The whole interferometric sequence takes place 100 μs after the condensate is released from the magnetic trap. In this way, we can both optimize the magnetization axis by carefully setting the magnetic bias field $\mathbf{B}$ and reduce the dissipative scattering due to the lower density of the cloud when illuminated by the Raman excitation beams. Moreover, in such a short time we are sure that the condensate neither exceeds the beam size nor evades the beam (the $1/e$ Raman beam diameter is approximately 50 μm, while the initial condensate size is below 5 μm).

The Raman pulse is formed by two spectral components separated in frequency by the Zeeman splitting for adjacent sub-levels (see Fig. 1(b)), and whose polarizations are set to σ and π with respect to the magnetization axis. Since the differential AC Stark shift between successive sub-levels induced by the out-of-resonance light is the same over the whole manifold, the Raman coupling is equally resonant with all the couples of adjacent Zeeman sub-levels, thus perfectly emulating the effect of an RF pulse.

The set-up is sketched in Fig. 2. The two light beams required for the transition are obtained from the same coherent source. They are sent to two different AOMs driven by two outputs of a single direct digital syntetizer (DDS). In this way the relative phase noise between the two Raman pulse components is reduced to the contribution given by their differential optical path, which is relevant on the time scale of the experimental sequence (30 s), while it is negligible on the time scale of a Raman pulse. The two beams are then made collinear and their polarizations orthogonal by means of a polarizing beam splitter (PBS1 in Fig. 2).

We note that by using co-propagating beams the momentum transferred to the atoms is limited to the negligible amount induced by the frequency difference of the beams. In our case, considering the Zeeman splitting $\Delta E = 2171$ kHz, it is $\Delta p = \hbar(k_1 - k_2) = \hbar\Delta\omega/c < 10^{-35}$ kg m/s (the magnetic field amplitude is set to ca. 3 G in order to minimize the quadratic Zeeman shift [16]). In these conditions, both the spatial phase modulation and the displacement induced by the momentum imprinted to the atomic wave packets are negligible, keeping a fringe contrast close to one. Moreover, large bandwidth of the Raman pulse ($1/\tau' \sim 100$ kHz) assures the conservation of the total energy for a large number of successive transitions.

The amplitude of the bias magnetic field $\mathbf{B}$ (present during the free fall of the samples until the application of the magnetic gradient) has been accurately measured by means of RF spectroscopy and evaluated as to $|\mathbf{B}| \sim 3.1$ G (corresponding to the Zeeman shift $\Delta E/\hbar = (2.171 \pm 0.02)$ MHz).

The calibration of the Raman pulses is provided by performing a Stern-Gerlach analysis after the application of a single pulse. In this way we can determine the applied pulse area from the observed population distribution, and find the coupling for which the sensitivity of the 5-state interferometer is maximized. Indeed, we know from [13] that the optimal pulse area is the one which gives a population distribution centered on the Zeeman sub-level $|F=2,m_F=0\rangle$. With the light coupling, this result is obtained for a pulse of duration $\Delta t = 6.2$ μs and measured power before the vacuum cell of 140 μW (π) and 280 μW (σ) (which corresponds to field intensities of 1.8 W/cm^2 (π) and 3.6 W/cm^2 (σ); beam waists $w_0 \sim 50$ μm).

#205748 - $15.00 USD Received 29 Jan 2014; revised 3 Apr 2014; accepted 5 Apr 2014; published 31 Jul 2014

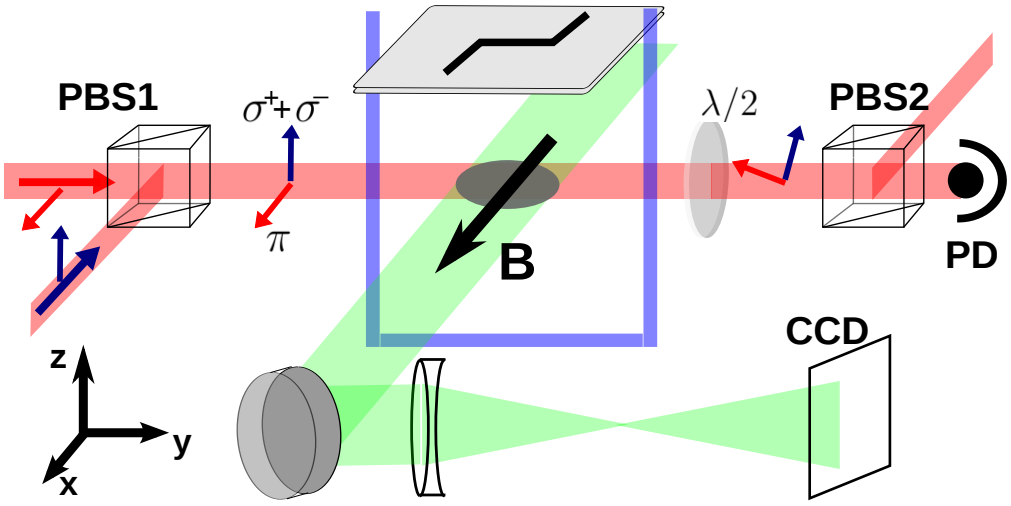

Fig. 2. Scheme of the experimental set-up. The generation of the Raman beams is obtained by merging two beams (red) on a polarizing beam-splitter (PBS1). The magnetization axis of the sample is set parallel to one of the two linear polarizations outgoing the PBS1, which is hence seen by the atoms as π-polarized, while the orthogonal one is seen as a sum of the opposite σ polarizations. Due to the Zeeman splitting induced by the bias magnetic field **B**, the component of the beam with the "wrong" σ polarization is out of resonance for the two-photon transition. After passing through the vacuum cell (blue), the two polarization components are mixed by means of a half-waveplate ($\lambda/2$) and a second polarizing beam-splitter (PBS2). This operation enables the detection of a beat note on the photodiode detector (PD) which reproduces the frequency difference and the relative phase between the two components. Both the magnetic trap and the Stern-Gerlach gradient are obtained by the same current-carrying z-shaped wire on the chip [13]. The absorption imaging beam is shown in green.

To determine the phase of the atomic coherence created by the Raman excitation, the two beams are sent onto a photodiode placed just after the vacuum cell, and the resulting beat note signal is recorded for each realization of the experiment. This beat note is then compared to a digital reference wave at the same frequency, synchronized with the time base of the experimental sequence. The phase read in this way is univocally related to the one seen by the atoms. Due to the 138 m scale of the differential wavelength associated with the two beams, length fluctuations in a few-centimeter path separating the detector from the vacuum cell can give only negligible contribution to the phase of the detected beat note.

In order to determine the response of the atoms to an RF pulse over the whole 2π range of possible Raman phases, the relative phase between the two fields is left free to evolve, so that due to mechanical, thermal, and electronic fluctuations and drifts, it randomly spans the complete 2π interval. By recording the results of the Stern-Gerlach analysis for a sufficiently high number of repetitions of the experiment it is hence possible to get a complete statistics concerning the dependence of the population distribution created by the Raman phase. The graphs of Fig. 3 are obtained after a binning operation on the detected phases: the 2π range has been divided into a number of segments, from the data points in each bin the mean population probabilities of the individual segments and their standard deviations have been determined.

In Fig. 3(a) we present the population distribution as a function of the Raman phase. For clarity, the fraction detected in each internal state (number of atoms in that state normalized

#205748 - $15.00 USD Received 29 Jan 2014; revised 3 Apr 2014; accepted 5 Apr 2014; published 31 Jul 2014

to the overall number of atoms) is shown separately and in individual colors. Additionally, we include in all the panels the results of the numerical simulations of the experiment (details on it below in the text). It is evident that the output of the interferometer is strongly correlated to the relative phase between the two fields which have crossed the sample. In particular, we determine a fringe resolution equal to (3.5 ± 0.4) on the detection of the Raman phase, 1.75 times higher than the theoretical limit for the ideal two-path case. The fringe narrowing is achieved without compromising the fringe contrast. Indeed, with this setup we are able to attain, for the $m_F = \pm 2$ states, the contrast close to unity required to obtain the theoretical maximal sensitivity (see Figs. 3(a) and 3(b); contrast is defined as $(\max - \min)$, where max and min are the maximum and the minimum of the fringe respectively). It means that the chosen detuning from resonance, about 18 GHz $\sim 3000\,\Gamma$ (with $\Gamma = 6$ MHz natural linewidth for the $D2$ line of Rb), is sufficient to reduce the incoherent scattering related to the Raman excitation to a negligible effect (the exploited coherent source is an extended cavity diode laser).

The three graphs of Fig. 3(b) are at different time delays T between the Raman and RF pulses, $T = 1.3; 1.4; 1.7$ μs from top to bottom respectively. Exploiting this degree of freedom it is possible to move the maximal slope of the fringes (and hence the maximal resolution) from one phase region to another one.

In Fig. 3(c) we report the detected fringe contrast in the $m_F = \pm 2$ states as a function of the delay time T. The solid line is a fit to the data obtained for an exponential decay function ($A \cdot e^{-t/\tilde{t}}$). The experimentally determined decay of the fringe contrast is reasonably well described by this function with maximal contrast $A = (0.88 \pm 0.02)$ and time constant $\tilde{t} = (61 \pm 9)$ μs. We identified the noise in the magnetic bias field as the main cause of the observed decay. Population decay is not present due to the fact that only sub-levels of the ground state are populated.

In Figs. 3(a) and 3(b) numerical simulations are also reported (solid lines). The population distribution is obtained by the numerical evaluation of the Schrödinger equation for the density matrix $\bar{\rho} : \partial_t \bar{\rho}(t) = -i[H(t), \bar{\rho}(t)] + L(t)$, where $H(t)$ is the Hamiltonian which generates the transfer matrix of Eq. (2), and we have added a Lindblad operator $L(t)$ to take into account decay rates (see [13] for details on the form of the Hamiltonian). Since we are dealing with atomic ground states, we have chosen $L(t)$ as an hollow matrix $L(t) = -4\pi\,\gamma\,[\bar{\rho}(t) - \mathrm{diag}(\bar{\rho}(t))]$ in order to restrict the decay to decoherence effects. A qualitative fit between data and the model is obtained assuming a value of γ between 1.0 kHz and 1.5 kHz (corresponding to the shaded area in Fig. 3(c)). Even if it is evident from the graph that a single exponential decay is not the correct expression for the evolution of the fringe contrast and there is no simple description of its decay, this representation is sufficient to determine the working time scale of this phase storage device.

For clarity, we would like to stress that our protocol is not a reproduction of the Ramsey procedure. Ramsey spectroscopy is obtained by repetition of the experimental sequence at fixed "interrogation" time T (the time interval separating the two pulses) while scanning the frequency of the radiation. The result is a fringe structure in the population distribution as a function of the excitation frequency. For longer interrogation time T, the fringes get narrower and closer, with an enhancement of the attainable sensitivity.

Here we have explored a different, technically simpler, configuration, in which the frequency of the radiation is maintained fixed and the sequence is repeated while changing the relative phase between the two pulses. In this case, the sensitivity is defined by the the maximum slope of the population distribution. For any value of the Raman phase, sensitivity of the interferometer can be set to maximum by choosing the appropriate delay time T. The maximum sensitivity is determined by the number of Zeeman states in the manifold.

#205748 - $15.00 USD Received 29 Jan 2014; revised 3 Apr 2014; accepted 5 Apr 2014; published 31 Jul 2014

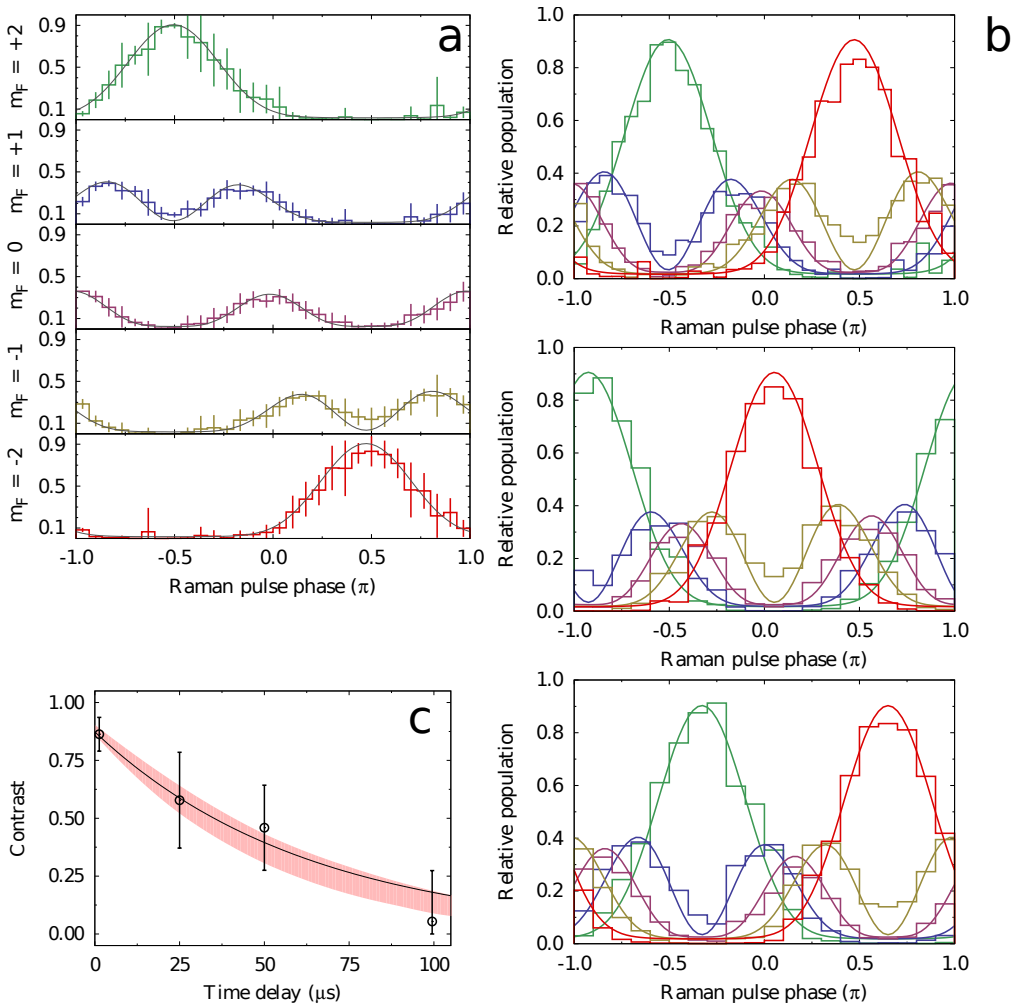

Fig. 3. Experimental results: **a)**, **b)** - population distribution as read at the output of the interferometer versus beat note phase read by the photodiode (histograms). In **a)** the internal state populations are separately shown for the five Zeeman states at delay $T = 1.3\ \mu$s. For the stretched states ($m_F = \pm 2$), the maximum slope we achieve is (0.64 ± 0.07) [rad]$^{-1}$. In **b)** population distribution for different interrogation time $T = 1.3; 1.4; 1.7\ \mu$s (from top to bottom respectively) are reported. By changing the delay time T between the two pulses it is possible to shift the phase region for which the maximum sensitivity is obtained. The periodicity of the fringe shift is given by the fundamental frequency of the system, that is the Zeeman splitting $\Delta E/\hbar = 2.171$ MHz. In all the graphs, solid lines represent population distributions obtained by numerical calculation of the evolution of the initial state in the density matrix representation.We have reported the results obtained for the decay rate $\gamma = 1$ kHz. **c)** - fringe contrast in the $m_F = \pm 2$ states as function of the time delay T. Fitting the data with an exponential decay (solid line) we obtain a decay time constant of $\tilde{t} = (61 \pm 9)\ \mu$s, which is in qualitative agreement with the trend predicted by the numerical simulations. The shaded area encloses the trend for decay rates γ between 1 kHz and 1.5 kHz ($\gamma = 1$ kHz $\rightarrow \tilde{t} \sim 75\ \mu$s, $\gamma = 1.5$ kHz $\rightarrow \tilde{t} \sim 50\ \mu$s).

#205748 - $15.00 USD Received 29 Jan 2014; revised 3 Apr 2014; accepted 5 Apr 2014; published 31 Jul 2014

4. Conclusions

We have demonstrated by means of atom interferometry the direct detection of the phase of an atomic coherence created in a degenerate bosonic sample via Raman coupling. The phase is written onto the atoms using a bichromatic coherent light field connecting the Zeeman substates of the $F = 2$ hyperfine level of ^{87}Rb Bose condensed atoms. The Raman pulse acts as the first beamsplitter of the interferometer. The phase is read out by an RF pulse acting as the second beamsplitter that closes the interferometer. The findings evidence that it is possible to store a phase information onto a degenerate atomic sample using all-optical means and to retrieve this information tenths of microseconds later without optical means.

An extension of the present experiment would be the use of nonclassical light states to prepare input states of a linear atom interferometer, hence bypassing the need for controllable atomic interactions. Atom interferometers of this kind are suitable for applications in quantum metrology.

Acknowledgments

This work was supported by the Seventh Framework Programme for Research of the European Comission, under FET-Open grant MALICIA (265522) and by MIUR under FIRB "Futuro in Ricerca" project HYTEQ and MAE under bilateral Serbia-Italy project M01049. P.L. and F.M. acknowledge support from ERA-NET CHIST-ERA (QScale). J.P. acknowledges support from the Ministry of Education, Science and Technological Development of Serbia, Project III 45010 and from LASERLAB-EUROPE (284464, EC FP7). We thank M. Inguscio for fruitful discussions and continuous support. We wish to thank M. Schramböck (Atominstitut, TU-Wien) at the ZMNS (TU-Wien) for the realization of the atom chip.

#205748 - $15.00 USD Received 29 Jan 2014; revised 3 Apr 2014; accepted 5 Apr 2014; published 31 Jul 2014